Structural phase transition and superconductivity in 2H-BaGaGe with buckled honeycomb layers

Dorota I. Walicka,[1,2,*] Robin Lefèvre,[2] Olivier Blacque,[2] Sara A. López-Paz,[1] Carl W. Rischau,[1] Antonio Cervellino,[3] Carlos A. Triana,[2] and Fabian O. von Rohr[1,†]

[1]*Department of Quantum Matter Physics, University of Geneva, CH-1211 Geneva, Switzerland*
[2]*Department of Chemistry, University of Zurich, CH-8057 Zurich, Switzerland*
[3]*Laboratory for Synchrotron Radiation - Condensed Matter, Paul Scherrer Institut, CH-5232 Villigen, Switzerland*

(Received 22 May 2023; accepted 7 July 2023; published 28 July 2023)

We report on the structural and superconducting properties of the intermetallic compound BaGaGe. We find that this material undergoes a structural second-order phase transition from a distorted AlB_2-type structure [1H, $a = 4.3254(2)$ Å, $c = 5.1078(3)$ Å, $P6/mmm$] into a $CaIn_2$-type structure [2H, $a = 4.3087(3)$ Å, $c = 10.2117(6)$ Å, $P6_3/mmc$] at a transition temperature of $T_S = 253$ K. We find that the structural phase transition corresponds to a coherent buckling of the honeycomb layers, which we can interpret as a disorder-to-order transition of the atoms located within this layer. We show that the 2H-BaGaGe phase becomes superconducting at a critical temperature of $T_c = 2.1$ K. The bulk nature of the superconductivity in 2H-BaGaGe is confirmed by means of specific-heat measurements, where we determine a value of $\Delta C/\gamma T_c = 1.59$, which is close to the expected BCS value in the weak-coupling limit.

DOI: 10.1103/PhysRevMaterials.7.074805

I. INTRODUCTION

Superconductivity in AlB_2-type compounds with honeycomb layers has been widely studied since the discovery of superconductivity with a critical temperature of $T_c = 39$ K in MgB_2 [1]. Prominent examples of the superconductivity on the honeycomb structure include the proposal for intrinsic topological superconductivity in SrPtAs [2–4], as well as superconductivity in magic-angle bilayer graphene [5].

There is a wide range of structural derivatives related to the AlB_2 structure with honeycomb layers. The main difference between these structures is the arrangement of the atoms within the honeycomb layers, the stacking sequences of the layers, as well as the buckling of the layers. Especially in ternary compounds, group-subgroup relationships lead to, among others, compounds with ZrBeSi-, $CaIn_2$-, and YPtAs-type structures [6]. Surprisingly, among over the ≈ 615 known intermetallic compounds in these structure types [7], only a few have been found to be superconducting [2–4,8,9].

The compound CaAlSi has the highest critical temperature among all reported ternary AlB_2-type superconductors, with a $T_c = 7.8$ K [10]. It crystallizes into the $P6_3/mmc$ space group with a so-called 6H structure. This structure contains six hexagonal layers of six-membered rings of $[AlSi]^{2-}$ units in its unit cell. These honeycomb layers are stacked on top of each other, and all of them are slightly buckled. Recently, it was reported—by means of specific-heat measurements and muon spin rotation spectroscopy—that the buckling of the layers seems to be correlated to an enhancement of the superconducting critical temperature in the $Ca_{1-x}Sr_xAlSi$ solid solution [9].

MgB_2 and the ternary nine-electron 111 systems are both considered to be conventional superconductors with electron-electron pairs mediated by phonons. However, the mechanisms of their electron-phonon coupling are believed to be notably different. In the case of MgB_2, the superconducting characteristics can be attributed to the partially filled B-B bonding states that exhibit a strong connection to the in-plane boron vibrations [11,12], while, for example, in the case of CaAlSi, theoretical analyses have pinpointed the partially filled π^* combined with an ultrasoft mode linked to the out-of-plane Al-Si vibration, as the potential foundation for the superconductivity [13].

Nine-electron 111 compounds with honeycomb layers can be considered as charge-imbalanced Zintl phases [14,15]. The ideal electronic structure of a planar hexagonal layer of these compounds leads to two π bands, one of which is bonding, while the other one is antibonding. Buckling of these honeycomb layers destroys the π bands and creates lone pairs in the electronic states, while at the same time, the soft mode that is responsible for the buckling of the layers is believed to be connected to the superconductivity of these compounds (see, e.g., Ref. [13]). Generally, in nine-electron 111 compounds with honeycomb layers, the superconductivity is the result of a complex interplay among various factors. These include the interrelationship of the structural elements, the associated phonon modes, the ensuing electronic modifications, and the cumulative impact of these aspects on superconductivity.

Within this family of compounds, BaGaGe was first reported to crystallize into a YPtAs-type structure [16], however, further studies have shown that it crystallizes in an AlB_2-type, i.e., 1H structure with planar honeycomb layers [14,17]. Preliminary data on 1H-BaGaGe suggested a

*dorota.walicka@unige.ch
†fabian.vonrohr@unige.ch

transition to a superconducting state at a critical temperature of $T_c = 2.4$ K [14].

In this paper, we study the structural and physical properties of BaGaGe. Specifically, we show that BaGaGe crystallizes in a distorted version of the AlB_2-type structure (1H) with buckled honeycomb layers and a statistical disorder around a mirror plane perpendicular to the c axis and that it undergoes a structural phase transition from a 1H to a 2H-type structure at $T_S \approx 253$ K, which corresponds to a coherent buckling in favor of one direction of the honeycomb layers. We find that this 2H-BaGaGe compound then undergoes a transition to a bulk superconducting state at low temperatures, which we characterize by means of resistivity, magnetization, and specific-heat measurements, providing a comprehensive overview of the physical properties.

II. METHODS

Synthesis. BaGaGe was prepared by arc melting under argon of stoichiometric amounts of Ba (Sigma Aldrich, 99.99%), Ga (Roth, 99.999%), and Ge (Alfa Aesar, 99.999%). The arc melting was performed on a water-cooled copper plate using a tungsten tip. The sample was flipped over and made completely molten three times, to ensure homogeneity, while avoiding evaporation of the elements. After arc melting the sample was sealed in a quartz tube (9 mm diameter) and annealed at 830 °C for 24 h, followed by cooling down to room temperature at a rate of 30 °C/h.

Diffraction. Temperature-dependent single-crystal x-ray diffraction (SXRD) measurements were collected using Cu $K\alpha_1$ ($\lambda = 1.54184$ Å) radiation with a XtaLAB Synergy, Dualflex, Pilatus 200K. The measured temperatures are listed in Tables S1–3 in the Supplemental Material [18]. Pre-experiment, data collection, manual data reduction, and absorption corrections were carried out with the program suite CRYSALISPRO [19]. Using the OLEX2 crystallography software [20], the structure was solved using the SHELXT intrinsic phasing solution program [21] and refined with the SHELXL 2018/3 program [22] by full-matrix least-squares minimization on F^2.

Temperature-dependent synchrotron powder x-ray diffraction (PXRD) experiments were carried out at the Swiss Light Source (SLS) at the Paul Scherrer Institute (PSI), Villigen, Switzerland, at the Materials Science (MS) X04SA beamline. The wavelength $\lambda = 0.563270(6)$ Å was refined using a LaB_6 standard. Measurements in the temperature range from 4.2 to 298 K were performed on a powdered sample filled in a 0.3-mm glass capillary. Data were analyzed by means of Rietveld refinement using the FULLPROF program suite [23].

Thus, we used single-crystal XRD to track the evolution of the crystal structure of our BaGaGe samples down to 100 K, and complementarily we used synchrotron powder XRD to reach temperatures as low as 4.2 K. This allowed us to confirm the accuracy of the solutions obtained from the single-crystal XRD analysis and further resolve the crystal structure of BaGaGe for temperatures below 100 K.

Elemental analysis. Elemental characterization was performed using a Zeiss GeminiSEM 450 field emission scanning electron microscope equipped with an x-ray detector X-MAX80, AZTec Advanced, Oxford. A total of ten spectra was collected at an applied voltage of 30 kV and at a 12 mm working distance.

Physical properties. The temperature-dependent magnetization measurements were performed using a Quantum Design Magnetic Properties Measurement System (MPMS3) equipped with a vibrating sample magnetometry (VSM) option and a 7 T magnet. Resistivity and specific heat were measured using a Quantum Design Physical Property Measurement System (PPMS) with a ^{3}He option for measurement below 1.8 K. For resistivity measurements the four-probe method was applied, where golden wires were connected to the sample with silver paste. Heat capacity measurements in a temperature range between $T = 1.8$ and 200 K were performed with the use of N Apiezon grease, while H Apiezon grease was used for the measurements between $T = 200$ and 300 K.

III. RESULTS AND DISCUSSION

A. Structural characterization

Phase-pure silvery shiny samples of BaGaGe were obtained. The samples were found to be brittle, and could be easily broken into small crystallites. The stoichiometry of the synthesized compound was measured by an energy-dispersive x-ray spectroscopy (EDX) analysis and the average atomic weights were calculated to be Ba $34.03 \pm 0.38\%$, Ga $32.67 \pm 0.59\%$, and Ge $33.30 \pm 0.41\%$, which correspond to a composition of $Ba_{1.02}Ga_{0.98}Ge_{1.00}$, close to the target 111 ratio.

The structure of BaGaGe was solved by means of synchrotron PXRD between $T = 298$ and 4.2 K, and with SXRD in the temperature range between $T = 350$ and 100 K. The evolution of the structure of BaGaGe is summarized in Fig. 1, and we will discuss it in detail in the following.

Using SXRD, the structural phase transition that BaGaGe undergoes—from the 1H-type structure to the 2H-type structure—could be resolved in detail. The Ge and Ga atomic positions could not be sufficiently distinguished with x-ray diffraction due to the similar scattering factor (close atomic numbers). Hence, in our structural model, a mixed occupancy was used of each site, i.e., 50% of the total site occupancy by Ge and 50% by Ga. Previous reports on BaGaGe [14,17] had found that at room temperature it crystallizes into an AlB_2-type structure where the atoms with the honeycomb lattice occupy the 2d Wyckoff position, $x = 2/3$, $y = 1/3$, and $z = 1/2$. However, our structural model for BaGaGe at high temperature suggests a 1H structure with buckled honeycomb layers, where the Ga/Ge atoms are located at the 4h Wyckoff position $x = 2/3$, $y = 1/3$, and $z = 0.4647$.

Four representative refinements from SXRD data measured at temperatures of $T = 274$, 255, 253, and 100 K are summarized in Table I and the corresponding atomic positions are reported in Table II. The data of all the other measurements are provided in the Supplemental Material (SM) [18]. From 350 down to 255 K the 1H structure was resolved with a statistical disorder around the mirror plane perpendicular to the c axis, leading to a 50%/50% probability for the buckling of the Ga/Ge layers in one direction, as shown in Fig. 1(a). Below a temperature of $T = 255$ K we observe a structural

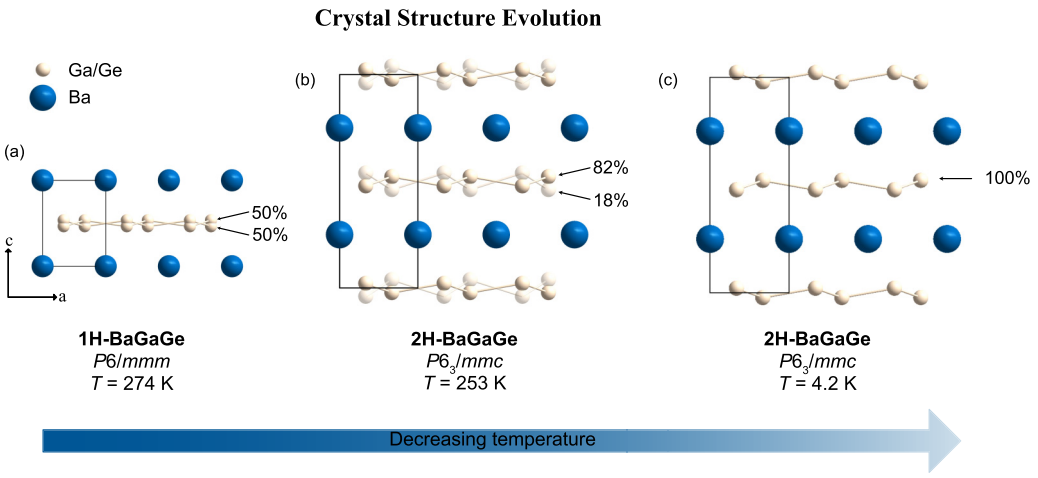

FIG. 1. Crystal structure of BaGaGe with varying temperature. (a) Structure from SXRD at 274 K: 1H modification with statistical disorder around the mirror plane perpendicular to the c axis leading to a 50%/50% probability of the buckling in one direction of the honeycomb lattice. (b) Structure from SXRD at 253 K: 2H modification with pronounced buckling, with a disorder site occupancy of 82%/18% in favor of one direction. (c) Structure from synchrotron PXRD at 4.2 K: fully ordered 2H structure.

phase transition, in which the buckling of the atoms is favored to face each other perpendicular to the c axis, which lowers the symmetry and causes doubling of the unit cell along the c axis. The refinement at a temperature of $T = 254$ K did not lead to a unique result for any of the two structures. However, the refinement at a so-called transition temperature $T_S = 253$ K clearly shows that the structure crystallizes in the $P6_3/mmc$ space group, with the full structural solution depicted in Fig. 1(b). At this $T_S = 253$ K the occupancy jumps from a 50%/50% probability of random order to a 82%/18% favored order. At the lowest recorded temperature using SXRD, i.e., $T = 100$ K, a 97% ordering of the buckling is found. Figure 2 shows the reconstruction of the reciprocal space along the

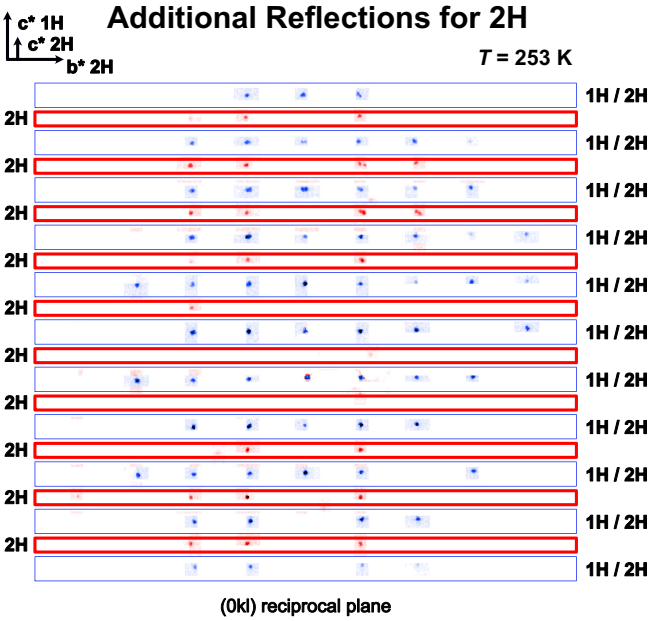

FIG. 2. Reconstruction of the reciprocal space along the $(0kl)$ reciprocal plane with additional reflections originating from the 2H-BaGaGe structure.

$(0kl)$ reciprocal plane, with additional reflections originating from the 2H structure. Refined unit cell parameters together with disorder site occupancies across the structural phase transition obtained from SXRD are summarized in Fig. 4(a).

To confirm the results obtained from SXRD, we performed synchrotron PXRD experiments. The differences between 1H and 2H structures are subtle, though clearly observable in the high-resolution synchrotron PXRD data. Hence, the Bragg reflections originating from the 2H structure could be conclusively resolved. In Fig. 3(a), we show three representative synchrotron PXRD patterns collected at temperatures of $T =$ 4.2, 195, and 298 K, along with the respective Rietveld refinements. Figures S1 and S2 in the SM [18] show the full set of synchrotron PXRD patterns. The cell parameters and agreement factors are summarized in Table S4 in the SM [18]. The Rietveld refinement of the synchrotron PXRD pattern collected at $T = 298$ K [see bottom of Fig. 3(a)] confirmed that BaGaGe crystallizes in the $P6/mmm$ space group. The 1H-BaGaGe structure remains a stable configuration for the temperature range from $T = 298$ to 256 K. Below T_S, the synchrotron PXRD patterns in the temperature range between $T = 254$ and 4.2 K display additional $(k0l)$ and (hkl) diffraction peaks, namely the (101), (105), (203), (205), (116), (213), (215), (101), (207), (313), (209), (402), (1011), (407), (317), and (1013) reflections. For clarity, the additional Bragg reflections with the highest intensities—originating from the 2H structure—are highlighted with arrows in the middle and top panels of Fig. 3(a). The intensity of these reflections progressively increases as we observe the disorder-to-order transition within the honeycomb lattice. An example of the intensity evolution of the (103) Bragg reflection is shown in Fig. 3(b). At base temperature, i.e., $T = 4.2$ K, the 2H structure is fully ordered. For visualization purposes, the structure of 2H-BaGaGe at a temperature of $T = 4.2$ K is depicted in Fig. 1(c).

The AlB_2 (1H) and $CaIn_2$ (2H) structure types are connected through a group-subgroup relation tree by a klassengleichen transformation [6]. This can be understood that both structures belong to the same class, but the unit cell has

TABLE I. Crystallographic data for single-crystal x-ray diffraction of BaGaGe at four different temperatures, with a transition observed around 254 K from the $P6/mmm$ to $P6_3/mmc$ space group.

Physical, crystallographic, and analytical data				
Formula	1H-BaGaGe	1H-BaGaGe	2H-BaGaGe	2H-BaGaGe
CCDC/FIZ	CSD-2263587	CSD-2263597	CSD-2263583	CSD-2263586
Structure type	AlB_2	AlB_2	$CaIn_2$	$CaIn_2$
Mol. wt. (g mol^{-1})	279.65	279.65	279.65	279.65
Crystal system	Hexagonal	Hexagonal	Hexagonal	Hexagonal
Space group	$P6/mmm$	$P6/mmm$	$P6_3/mmc$	$P6_3/mmc$
Space group number	191	191	194	194
a (Å)	4.3254(2)	4.32097(18)	4.3204(2)	4.3087(3)
b (Å)	4.3254(2)	4.32097(18)	4.3204(2)	4.3087(3)
c (Å)	5.1078(2)	5.1093(2)	10.2199(5)	10.2117(6)
V (Å^3)	82.759(8)	82.615(8)	165.206(17)	164.18(2)
Z	1	1	2	2
Calculated density (g cm^{-3})	5.611	5.621	5.622	5.657
Data collection				
Temperature (K)	274(6)	255.00(10)	253.00(10)	99.9(2)
Radiation	Cu $K\alpha_1$ (1.54184 Å)	Cu $K\alpha_1$ (1.54184 Å)	Cu $K\alpha_1$ (1.54184 Å)	Cu $K\alpha_1$ (1.54184 Å)
Crystal color	Gray shiny			
Crystal size (mm^3)	0.02 × 0.02 × 0.01	0.02 × 0.01 × 0.01	0.02 × 0.02 × 0.01	0.02 × 0.01 × 0.01
Linear absorption coefficient (cm^{-1})	1092.08	1093.99	1094.15	1100.98
Scan mode	ω	ω	ω	ω
Recording range θ (deg)	8.681–73.059	11.844–77.012	8.677–66.656	8.684–66.879
h range	−4 to +5	−5 to +3	−5 to +4	−4 to +4
k range	−5 to +5	−3 to +5	−5 to +4	−5 to +3
l range	−5 to +6	−6 to +6	−9 to +12	−10 to +12
No. of measured reflections	463	472	825	812
Data reduction				
Completeness	100	100	100	100
No. of independent reflections	55	55	76	76
R_{int} (%)	2.38	2.46	2.89	3.56
Absorption corrections	Sphere	Sphere	Sphere	Sphere
Empirical corrections	Frame scaling and spherical harmonics			
Independent reflections with $I \geqslant 2.0\sigma$	55	55	69	72
Refinement				
R_1 (obs/all) (%)	1.24/1.24	0.94/0.94	0.94/1.10	0.98/1.23
wR_2 (obs/all) (%)	2.61/2.61	2.27/2.27	1.83/1.85	2.33/2.39
GOF	1.310	1.215	1.079	1.185
No. of refined parameters	7	7	8	8
Difference Fourier residues (eÅ^{-3})	−0.354/ + 0.332	−0.370/ + 0.455	−0.295/0.247	−0.259/0.477

to be enlarged for the 2H structure, which also reduces other symmetry elements, i.e., the sixfold rotation axis is replaced with a 6_3 screw axis and the mirror plane m is replaced by a c axial glide plane. The unit cell transformation and shift of the origin are shown in Fig. 3(c). The phase transitions between space groups connected by the group-subgroup relationships are usually of a second order [24], with a progressive conversion over a certain temperature range. Here, in the case of BaGaGe, this can be very well illustrated when observing the evolution of unit cell parameters within one layer as depicted in Fig. 4(b). We find the cell parameter a to decrease over the whole temperature range with decreasing temperature, as expected by the thermal expansion. The cell parameter c has a more complex change as it is featuring the structural phase transition. The cell parameter c first increases with decreasing temperature due to the progressive buckling of the honeycomb layers, which increases the interlayer distance. Then, below $T \approx 180$ K, the cell parameter c decreases with decreasing temperature as expected. A slow, progressive change of the cell parameter c over a large temperature range confirms the second-order nature of the 1H to 2H phase transition.

B. Physical properties

The temperature-dependent resistivity of BaGaGe in the temperature range between $T = 300$ and 1.8 K in zero magnetic field $\mu_0 H = 0$ T is depicted in Fig. 5(a). The resistivity of BaGaGe decreases with decreasing temperature,

TABLE II. Refined coordinates, iso- and anisotropic displacement parameters (ADPs), and their estimated standard deviations for a temperature study of the single-crystal x-ray diffraction of BaGaGe. The Ga/Ge ratio was always fixed to 50/50 on each shared position as x-rays do not allow to distinguish Ga/Ge atoms. $U_{11} = U_{22} = U_{13}$, $U_{23} = 0$ due to symmetry constraints.

T (K)	Space group	Atom	Wyckoff	Occ.	x	y	z	U_{iso}	U_{11}	U_{33}	U_{12}
274	$P6/mmm$	Ba	1a	1	0	0	0	0.0228(3)	0.0231(3)	0.0223(4)	0.01153(17)
		(Ga/Ge)	4h	0.50	2/3	1/3	0.4647(13)	0.291(11)	0.0211(5)	0.045(3)	0.0106(3)
255	$P6/mmm$	Ba	1a	1	0	0	0	0.0147(3)	0.0150(3)	0.0140(4)	0.00750(14)
		(Ga/Ge)	4h	0.50	2/3	1/3	0.4619(8)	0.0196(8)	0.0129(4)	0.033(3)	0.00646(18)
253	$P6_3/mmc$	Ba	2b	1	0	0	3/4	0.0132(2)	0.0135(2)	0.0125(3)	0.00676(12)
		(Ga/Ge)1	4f	0.82	1/3	2/3	0.48145(8)	0.0185(3)	0.0117(3)	0.0322(7)	0.00583(14)
		(Ga/Ge)2	4f	0.18	1/3	2/3	0.5219(6)	0.0185(3)	0.0117(3)	0.0322(7)	0.00583(14)
99.9	$P6_3/mmc$	Ba	2b	1	0	0	3/4	0.0120(3)	0.0123(3)	0.0115(4)	0.00617(15)
		(Ga/Ge)1	4f	0.97	1/3	2/3	0.47832(4)	0.0157(3)	0.0117(4)	0.0237(5)	0.00586(18)
		(Ga/Ge)2	4f	0.03	1/3	2/3	0.5237(15)	0.0157(3)	0.0117(4)	0.0237(5)	0.00586(18)

displaying a metallic behavior. At the structural phase transition $T_S = 253$ K a clearly pronounced discontinuity is observed, which is highlighted with an arrow in Fig. 5(a). We find a residual resistivity ratio (RRR) for the 2H-BaGaGe, here defined as RRR $= \rho(225\text{ K})/\rho(3\text{ K}) = 1.54$, which indicates a short mean free path of the charge carriers, i.e., a bad-metal behavior. This value for the RRR is likely associated with the polycrystalline nature of the sample that was measured, and henceforth with the significant contribution of the grain boundaries to the sample's resistivity. At low temperatures, we observe a sharp drop in the resistivity at the transition to the superconducting state. We determine the critical temperature to be $T_c = 2.1$ K at a 50% decrease of $\rho(T)$ from the resistivity [Fig. 5(a) inset].

In the temperature-dependent magnetization measurements, we find that BaGaGe is a Pauli paramagnet in the

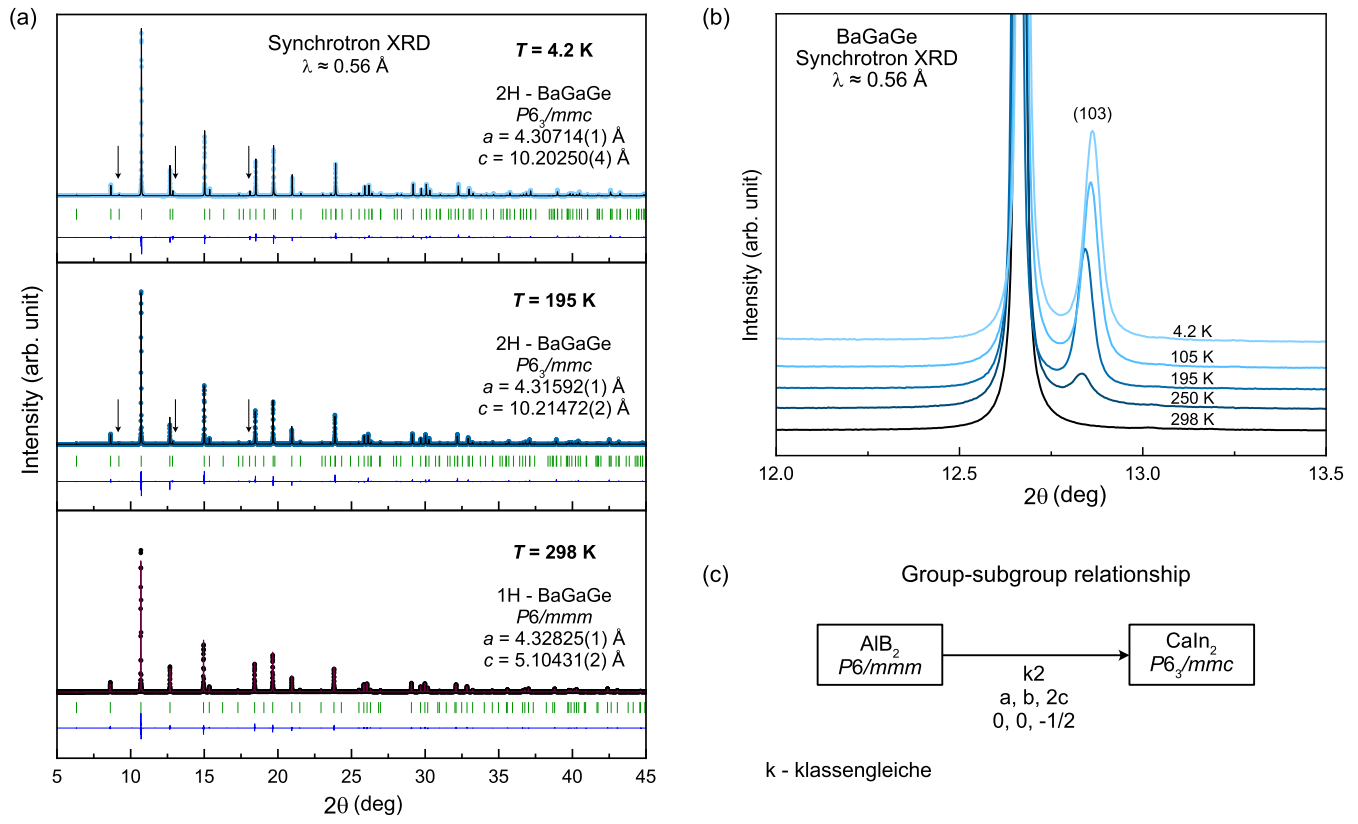

FIG. 3. (a) Rietveld refinement of the synchrotron PXRD patterns measured at $T = 4.2$, 195, and 298 K. The arrows indicate the position of selected additional peaks originating from the 2H structure. (b) Evolution of the (103) peak with the temperature from synchrotron PXRD. (c) Group-subgroup relationship between 1H-BaGaGe and 2H-BaGaGe. Below the arrow the index ($k2$), unit cell transformation ($a, b, 2c$), and origin shift $(0, 0, -1/2)$ are indicated.

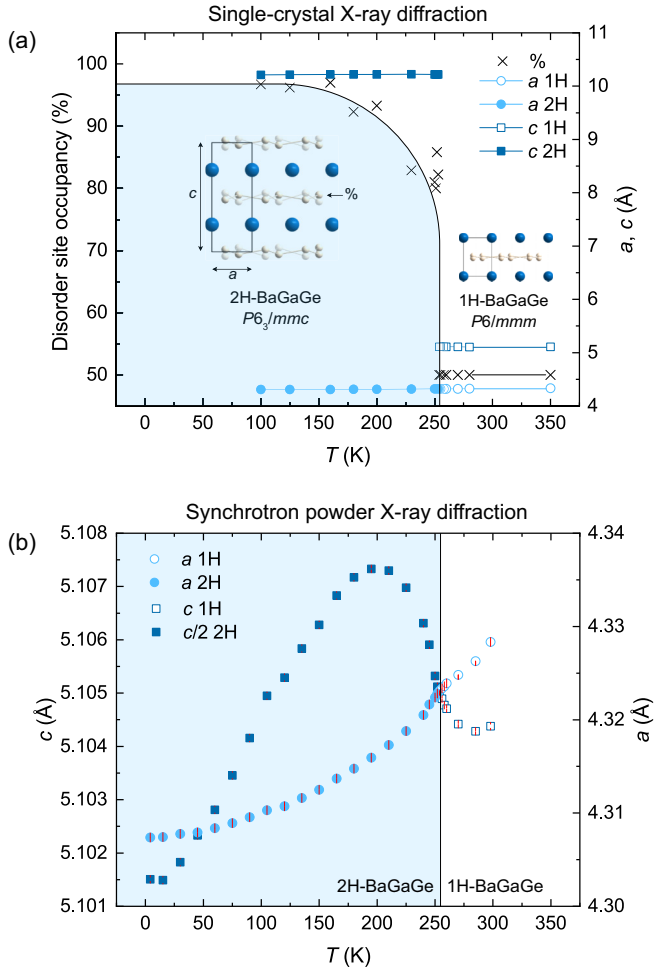

FIG. 4. (a) Unit cell parameters and disorder site occupancies from SXRD data. (b) Evolution of the unit cell parameters with temperature obtained from synchrotron PXRD. The c axis for the 2H-BaGaGe was divided by 2 for better comparability.

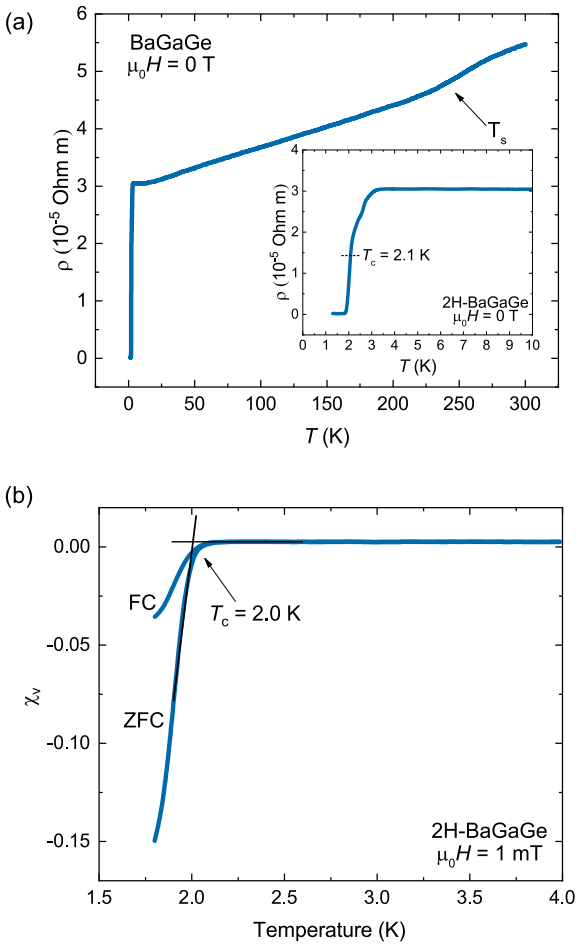

FIG. 5. (a) Resistivity data in the temperature range between $T = 1.3$ and 300 K. The inset shows the transition to the superconducting state with $T_c = 2.1$ K assigned at the 50% drop of $\rho(T)$. (b) Zero-field-cooling (ZFC) and field-cooling (FC) magnetization in the temperature range between $T = 1.8$ and 4 K in an external magnetic field of $\mu_0 H = 1$ mT, with $T_c = 2.0$ K in the magnetization.

normal state, with a nearly temperature-independent positive magnetization between $T = 300$ and 5 K (see Fig. S3 in the SM [18]) in magnetic fields of $\mu_0 H = 0.1$ and 1 T.

In order to characterize the superconducting state by magnetization, we have performed zero-field-cooled (ZFC) and field-cooled (FC) measurements in an external field of $\mu_0 H = 1$ mT, as shown in Fig. 5(b). The superconducting transition is clearly pronounced, with a strong diamagnetic shielding fraction. We determine the critical temperature to be $T_c = 2.0$ K in the magnetization.

In Figs. 6(a) and 6(b), we show the temperature-dependent heat capacity of BaGaGe in the superconducting state and in the normal state, respectively. The heat capacity data in the low temperatures [see Fig. 6(b) inset] were analyzed using the equation

$$C_p = C_{el} + C_{Debye}, \tag{1}$$

$$C_p/T = \gamma + \beta T^2, \tag{2}$$

which allowed us to determine $\gamma = 4.33(3)$ mJ mol^{-1} K^{-2} and $\beta = 0.321(2)$ mJ mol^{-1} K^{-1} for 2H-BaGaGe. The Debye temperature, i.e., the temperature of the highest normal mode of vibration, was derived from the β coefficient according to

$$\Theta_D = \left(\frac{12\pi^4}{5\beta} nR\right)^{1/3}, \tag{3}$$

where $n = 3$ and $R = 8.31$ J mol^{-1} K^{-1} is the gas constant. We obtain a Debye temperature of $\Theta_D = 263(1)$ K for 2H-BaGaGe.

The jump of the heat capacity corresponds to the transition to the superconducting state and arises from the difference of the specific heat of the electrons in the normal state and when combined in Cooper pairs. With the entropy conserving construction shown in Fig. 6(a) we find a critical temperature in the specific heat of $T_c = 1.89$ K. This value is—as expected—slightly lower than the critical temperatures in the resistivity and the magnetization measurements, and therefore in very good agreement with them. The value of $\Delta C/\gamma T_c = 1.59$ is slightly larger than the value expected for the weak-coupling

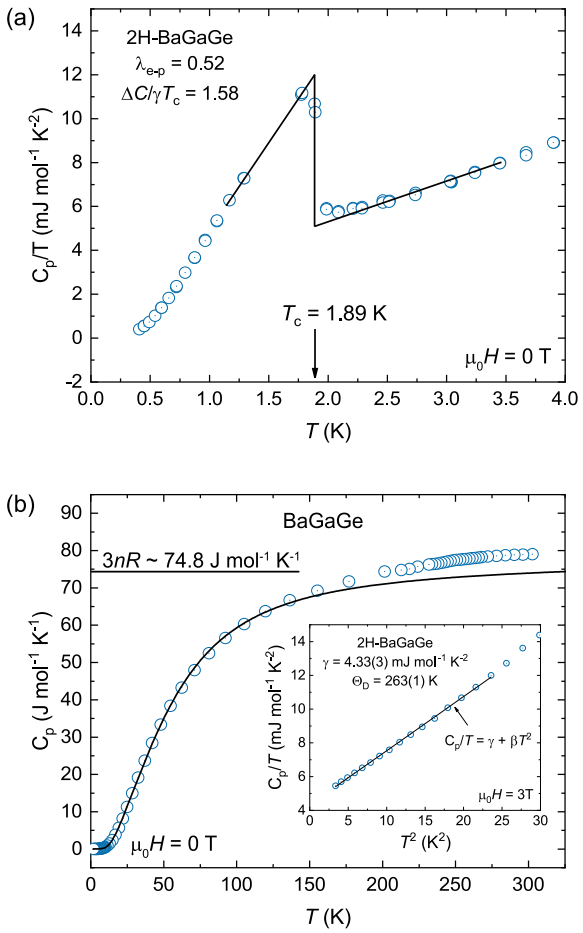

FIG. 6. (a) Temperature-dependent heat capacity of 2H-BaGaGe in the vicinity of the superconducting phase transition with an entropy-conserving construction. (b) Heat capacity data in the temperature range between $T = 300$ and 2 K. Inset: Heat capacity at low temperatures measured in a magnetic field of 3 T.

BCS theory of 1.43. The value is evidence for 2H-BaGaGe to be a bulk superconductor.

The obtained values for T_c and Θ_D allow us to estimate the electron-phonon coupling constant $\lambda_{e\text{-}p}$, for which we use the semiempirical McMillan formula [25]:

$$\lambda_{e\text{-}p} = \frac{1.04 + \mu^* \ln(\Theta_D/1.45T_c)}{(1 - 0.62\mu^*)\ln(\Theta_D/1.45T_c) - 1.04}. \quad (4)$$

Here, μ^* is the Coulomb pseudopotential parameter, and for our estimation, we have set $\mu^* = 0.13$. This is an average value used commonly for intermetallic superconductors (see, e.g., Refs. [9,26]). We find an electron-phonon coupling constant of $\lambda_{e\text{-}p} = 0.52$. This value is in good agreement, with 2H-BaGaGe being a superconductor in a weak-coupling limit. Furthermore, we find the electron density at the Fermi level from the Sommerfeld coefficient γ to be $D(E_F) = 1.21$ states eV^{-1}, by applying

$$D(E_F) = \frac{3\gamma}{\pi^2 k_B^2 (1 + \lambda_{e\text{-}p})}, \quad (5)$$

where $k_B = 1.38 \times 10^{-23}$ J K^{-1} is the Boltzmann constant.

The heat capacity data in the normal state of 2H-BaGaGe, i.e., below the structural phase transition, in a temperature range between $T = 200$ and 3 K was analyzed using an extension of Eq. (1),

$$C_p = C_{el} + C_{Debye} + C_{Einstein}, \quad (6)$$

where the total specific heat is a mixture of the electron (C_{el}) and phonon contribution (C_{Debye} and $C_{Einstein}$):

$$C_{el}(T) = \gamma T, \quad (7)$$

$$C_{Debye}(T) = 9nRk\left(\frac{T}{\Theta_D}\right)^3 \int_0^{\Theta_D} \frac{x^4 e^x}{(e^x - 1)^2} dx, \quad (8)$$

$$C_{Einstein}(T) = 3nR(1 - k)\left(\frac{\Theta_E}{T}\right)^2 \frac{e^{\Theta_E/T}}{(e^{\Theta_E/T} - 1)^2}. \quad (9)$$

Here, Θ_E is the Einstein temperature, k is a weight factor, and $\gamma = 4.33(3)$ mJ mol^{-1} K^{-2}, obtained from the low-temperature fit, was used. We obtain $\Theta_D = 257(9)$ K, $\Theta_E = 91(6)$ K, and $k = 0.73$. The fitting of Eq. (6) is shown in Fig. 6(b) as a black line. Above 100 K the data start to diverge from the fit due to the broad structural phase transition. The value of Θ_D is in very good agreement with the value obtained from the low-temperature data, as well as the value of the Θ_E additionally estimated to be 96 K (see Fig. S4 in the SM [18]). In agreement with the Dulong-Petit law, $C_p(T)$ data at high temperature approach a value of $3nR = 74.8$ J mol^{-1} K^{-1}, where n is the number of atoms per unit cell and $R = 8.31$ J mol^{-1} K^{-1} is the gas constant.

IV. SUMMARY AND CONCLUSION

In this paper, we have analyzed the structural and superconducting properties of BaGaGe. We have shown an improved model of the BaGaGe structure at high temperatures, where BaGaGe crystallizes in a distorted version of the AlB_2-type structure with buckled honeycomb layers and a statistical disorder around a mirror plane. Moreover, the compound undergoes a second-order structural phase transition from the 1H-BaGaGe structure to the 2H-BaGaGe structure with coherent buckling in favor of one direction, which we interpret as a disorder-to-order phase transition. We have investigated the details of the temperature evolution of the buckling of the honeycomb Ga/Ge layer by means of SXRD and synchrotron PXRD. We showed that the structural phase transition happens over an extended temperature range with a maximum at $T_S = 253$ K. The structural phase transition can also be understood as a doubling of the unit cell along the c axis as a consequence of a disorder-to-order phase transition in the honeycomb layer. By means of SXRD we have concluded that in the temperature range from 298 to 254 K the system displays 50%/50% positional disorder of Ga/Ge atoms while below 253 K the honeycomb layer starts to buckle in favor of one direction. At 253 K, we have observed a 82%/18% ratio of the electron density in favor of one direction, which progressively orders towards the fully buckled structure below 100 K. The synchrotron PXRD allowed us to confirm the presence of the 2H structure down to 4.2 K. We measured resistivity, magnetization, and specific heat in order to fully characterize the normal state as well as the superconducting properties of 2H-BaGaGe. All three measurements show that BaGaGe undergoes an electronic transition to a

bulk superconducting state with a critical temperature of $T_c = 2.1$ K. Furthermore, from the specific heat we have obtained a $\Delta C/\gamma T_c = 1.59$, which is close to the expected BCS value and is evidence for the bulk nature of the superconductivity in 2H-BaGaGe in the weak-coupling limit. We find BaGaGe to be a versatile honeycomb compound that displays superconductivity in the vicinity of a structural phase boundary.

ACKNOWLEDGMENTS

Energy-dispersive x-ray spectroscopy experiments were performed with equipment maintained by the Center for Microscopy and Image Analysis at the University of Zurich. This work was supported by the Swiss National Science Foundation under Grant No. PCEFP2_194183.

[1] J. Nagamatsu, N. Nakagawa, T. Muranaka, Y. Zenitani, and J. Akimitsu, Superconductivity at 39 K in magnesium diboride, Nature (London) **410**, 63 (2001).

[2] Y. Nishikubo, K. Kudo, and M. Nohara, Superconductivity in the honeycomb-lattice pnictide SrPtAs, J. Phys. Soc. Jpn. **80**, 055002 (2011).

[3] P. K. Biswas, H. Luetkens, T. Neupert, T. Stürzer, C. Baines, G. Pascua, A. P. Schnyder, M. H. Fischer, J. Goryo, M. R. Lees *et al.*, Evidence for superconductivity with broken time-reversal symmetry in locally noncentrosymmetric SrPtAs, Phys. Rev. B **87**, 180503(R) (2013).

[4] M. H. Fischer, T. Neupert, C. Platt, A. P. Schnyder, W. Hanke, J. Goryo, R. Thomale, and M. Sigrist, Chiral *d*-wave superconductivity in SrPtAs, Phys. Rev. B **89**, 020509 (2014).

[5] Y. Cao, V. Fatemi, S. Fang, K. Watanabe, T. Taniguchi, E. Kaxiras, and P. Jarillo-Herrero, Unconventional superconductivity in magic-angle graphene superlattices, Nature (London) **556**, 43 (2018).

[6] R.-D. Hoffmann and R. Pöttgen, AlB_2-related intermetallic compounds – a comprehensive view based on group-subgroup relations, Z. Kristallogr. **216**, 127 (2001).

[7] J. Dshemuchadse and W. Steurer, More statistics on intermetallic compounds – ternary phases, Acta Crystallogr., Sect. A **71**, 335 (2015).

[8] B. Lorenz, J. Cmaidalka, R. L. Meng, and C. W. Chu, Thermodynamic properties and pressure effect on the superconductivity in CaAlSi and SrAlSi, Phys. Rev. B **68**, 014512 (2003).

[9] D. I. Walicka, Z. Guguchia, J. Lago, O. Blacque, K. Y. Ma, H. Liu, R. Khasanov, and F. O. von Rohr, Two-gap to single-gap superconducting transition on a honeycomb lattice in $Ca_{1-x}Sr_xAlSi$, Phys. Rev. Res. **3**, 033192 (2021).

[10] M. Imai, E.-H. S. Sadki, H. Abe, K. Nishida, T. Kimura, T. Sato, K. Hirata, and H. Kitazawa, Superconducting properties of single-crystalline $Ca(Al_{0.5}Si_{0.5})2$: A ternary silicide with the AlB_2-type structure, Phys. Rev. B **68**, 064512 (2003).

[11] I. I. Mazin, O. K. Andersen, O. Jepsen, O. V. Dolgov, J. Kortus, A. A. Golubov, A. B. Kuz'menko, and D. van Der Marel, Superconductivity in MgB_2: Clean or Dirty?, Phys. Rev. Lett. **89**, 107002 (2002).

[12] H. J. Choi, D. Roundy, H. Sun, M. L. Cohen, and S. G. Louie, The origin of the anomalous superconducting properties of MgB_2, Nature (London) **418**, 758 (2002).

[13] I. I. Mazin and D. A. Papaconstantopoulos, Electronic structure and superconductivity of CaAlSi and SrAlSi, Phys. Rev. B **69**, 180512(R) (2004).

[14] M. J. Evans, Y. Wu, V. F. Kranak, N. Newman, A. Reller, F. J. Garcia-Garcia, and U. Häussermann, Structural properties and superconductivity in the ternary intermetallic compounds *MAB* (M = Ca, Sr, Ba; A = Al, Ga, In; B = Si, Ge, Sn), Phys. Rev. B **80**, 064514 (2009).

[15] M. Giantomassi, L. Boeri, and G. B. Bachelet, Electrons and phonons in the ternary alloy $CaAl_{2-x}Si_x$ as a function of composition, Phys. Rev. B **72**, 224512 (2005).

[16] A. Czybulka, B. Pinger, and H. Schuster, Neue erdalkali-gallium-silicide, -germanide und -stannide mit vom AlB_2-typ abgeleiteten strukturen, Z. Anorg. Allg. Chem. **579**, 151 (1989).

[17] M. J. Evans, G. P. Holland, F. J. Garcia-Garcia, and U. Häussermann, Polyanionic gallium hydrides from AlB_2-type precursors AeGaE (Ae = Ca, Sr, Ba; E = Si, Ge, Sn), J. Am. Chem. Soc. **130**, 12139 (2008).

[18] See Supplemental Material at http://link.aps.org/supplemental/10.1103/PhysRevMaterials.7.074805 for the crystallographic data for the single-crystal measurements; synchrotron PXRD patterns, corresponding Rietveld refinements, unit cell parameters and agreement factors; magnetic susceptibility in the temperature range from 5 to 300 K in the magnetic fields of 0.1 and 1 T; and lattice specific heat of BaGaGe.

[19] CrysAlisPro, Agilent Technologies UK Ltd., ver. 41 (2014).

[20] O. V. Dolomanov, L. J. Bourhis, R. J. Gildea, J. A. Howard, and H. Puschmann, OLEX2: A complete structure solution, refinement and analysis program, J. Appl. Crystallogr. **42**, 339 (2009).

[21] G. M. Sheldrick, SHELXT - Integrated space-group and crystal-structure determination, Acta Crystallogr., Sect. A **71**, 3 (2015).

[22] G. M. Sheldrick, Crystal structure refinement with SHELXL, Acta Crystallogr., Sect. C **71**, 3 (2015).

[23] J. Rodríguez-Carvajal, Recent advances in magnetic structure determination by neutron powder diffraction, Phys. B: Condens. Matter **192**, 55 (1993).

[24] U. Muller, *Inorganic Structural Chemistry* (Wiley, Hoboken, NJ, 2006).

[25] W. L. McMillan, Transition temperature of strong-coupled superconductors, Phys. Rev. **167**, 331 (1968).

[26] F. Von Rohr, M. J. Winiarski, J. Tao, T. Klimczuk, and R. J. Cava, Effect of electron count and chemical complexity in the Ta-Nb-Hf-Zr-Ti high-entropy alloy superconductor, Proc. Natl. Acad. Sci. USA **113**, E7144 (2016).